3rd EUROPEAN CONFERENCE ON
EARTHQUAKE ENGINEERING & SEISMOLOGY
BUCHAREST, ROMANIA, 2022

Preliminary seismic risk assessment of ancient columns across Attica for application in decision support systems

Christos G. Lachanas – School of Civil Engineering, National Technical University of Athens, Athens, Greece, e-mail: lahanasch@central.ntua.gr

Dimitrios Vamvatsikos – School of Civil Engineering, National Technical University of Athens, Athens, Greece, e-mail: divamva@mail.ntua.gr

Abstract: An approach for preliminary seismic risk assessment is presented for portfolios of cultural heritage assets of classical antiquity. As an example, three ancient columns are considered, located at different sites throughout Attica: The Temple of Aphaia in Aegina, the Temple of Olympian Zeus in the centre of Athens, and the Temple of Poseidon in Sounio. Event-based probabilistic seismic hazard analysis is used for the definition of the seismic hazard via multiple correlated intensity measure fields. The seismic response of the columns is assessed via simplified equations for the prediction of the central value and the dispersion of the lognormal fragility function for rocking blocks. Afterwards, the seismic risk per asset is assessed both in terms of long-term averages, calculating the mean annual frequency of exceeding pre-defined limit states, as well as on an event-by-event basis, calculating the probability of exceeding limit states of interest per asset in scenario events. Overall, a comprehensive tool is offered for supporting decision-making on prioritizing rehabilitation actions for a portfolio of monumental structures.

Keywords: seismic hazard, seismic risk, rocking blocks, decision support systems

1. Introduction

The protection of the cultural heritage assets against natural hazards is a crucial task that has raised the interest of researchers and society alike. After all, a society without cultural heritage will end up as a tree without roots and is thus doomed to wither. Attica is a distinctive example of a region where multiple cultural heritage assets are spread in close distances from each other. All these assets are exposed to the same seismic events but still each one is influenced to a different degree due to the spatial variability of the ground motion hazard (i.e., distance from the rupture, soil conditions, etc.) (Weatherill et al. 2015, Lachanas et al. 2022). Hence, in modern decision support systems (e.g., Pitilakis et al. 2014, Vamvatsikos et al. 2022), seismic risk assessment has shifted from tackling each asset and site on their own to treating simultaneously groups of assets on an event-by-event basis. This approach is useful for stakeholders since it can be used as a tool for the seismic risk assessment of a portfolio of distributed assets on a long-term basis, using stochastic sets of potential seismic events, as well as on a near-real-time basis when convolved with on-site real-time monitoring.

Aiming to provide a practical example, a set of cultural heritage sites of classical antiquity is considered in Attica, and a simple approach for assessing the ensemble seismic risk is presented. Three different monuments are investigated: The Temple of Aphaia in Aegina (Southwest Attica), the Temple of Olympian Zeus (centre of Athens), and the Temple of Poseidon in Sounio (Southeast Attica). In all cases, one single column per temple is adopted per site as the asset of interest. Rather than performing structural analysis, fragility functions are constructed via the expressions of Kazantzi et al. (2021), which provide the parameters of the lognormal fragility function for rocking blocks. The seismic risk per asset is offered both in terms of the long-term averages as well as under different potential scenario events of varying magnitudes and epicentre location.

2. Seismic hazard calculations

Event-based Probabilistic Seismic Hazard Analysis (PSHA, Weatherill et al. 2015) with spatial correlation (Jayram and Baker 2009) was employed to calculate the seismic hazard. This is performed by considering a stochastic event set of potential ruptures during a predefined time period on a one-by-one basis. Each event corresponds to an Intensity Measure (IM) field (Fig. 1). The OpenQuake open-source platform (GEM 2016) was used to perform the PSHA calculations for a grid of sites along Attica (Fig. 1) using the European seismic source model (ESHM13, Woessner et al. 2015). Of the available logic tree branches provided, only the area source model and the Boore and Atkinson (2008) ground motion prediction equation were employed. A uniform "rock" soil-type was assumed (V_{s30}=800m/s). The geomean (geometric mean of the two horizontal components) peak ground acceleration, PGA_{gm}, was employed as IM. An effective investigation period of 10,000 years was adopted; this was found by Lachanas et. al 2022 to be adequate for the case of Attica for calculating the Mean Annual Frequency (MAF) of exceeding PGA_{gm} ($\lambda_{PGA_{gm}}$) when compared to the classical PSHA approach (Cornell 1968, Bommer 2002). Fig. 2, presents the location on map of the three cultural heritage assets under investigation (Fig. 2a) and the corresponding hazard curves (Fig. 2b). As presented, seismic hazard is reduced when moving from West to East Attica. In addition, event-based PSHA for an investigation period of 10,000 years leads to hazard curves that match those of the classical approach within an acceptable range. In other words, both methods capture equally well the frequent events (low PGA_{gm} – high $\lambda_{PGA_{gm}}$) that mostly matter for assessing loss and damage, whereas for the rarer ones longer investigation periods are needed.

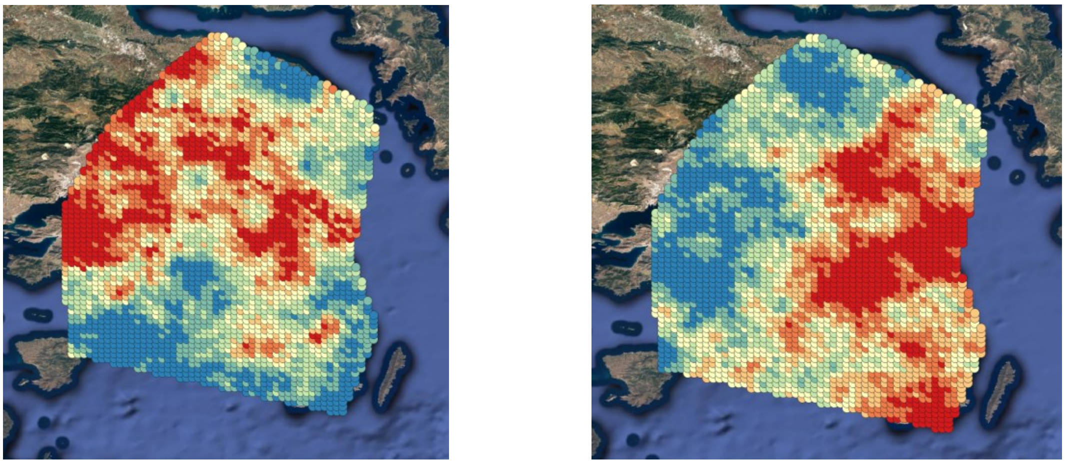

(a) (b)

Fig. 1 – Example of IM fields representing: a) a possible rupture in the Northwest and b) a possible rupture in the East (spectral colormap from red to blue referring to the higher to the lowest IM values per field) (map background from Google Earth, IM field plotted using QGIS)

(a)

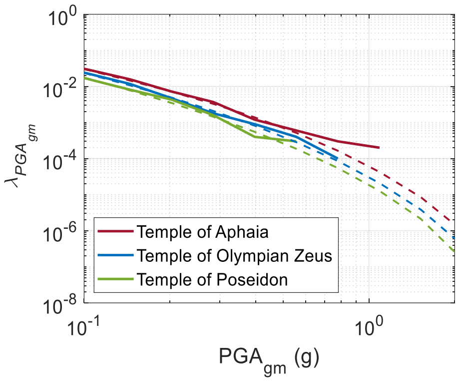

(b)

Fig. 2 – a) Location of the monuments under investigation (map background from Google Earth, location of the assets plotted using QGIS), b) Mean hazard curves for PGA_{gm} at the sites of interest (solid line: Event-based PSHA for an effective investigation period of 10,000 years, dashed lines: Classical PSHA)

3. Structural modelling

Fig. 3a presents the typical planar model of a rectangular rigid block standing freely on a rigid support base and subjected to horizontal excitation $\ddot{u}_g(t)$. The geometry of the block can be defined by the slenderness angle $\alpha = \tan^{-1}(2b/2h)$ and the half-diagonal $R = \sqrt{h^2 + b^2}$. Assuming that the coefficient of friction between the block's base and its support surface is high enough to prevent sliding, the block undergoes rocking when the horizontal acceleration is strong enough to trigger uplift. After uplift, the block rocks between its pivot points O-O'. Housner (1963) proposed the rocking equation of motion. Afterwards, many studies (e.g., Yim et. al 1980, Ishiyama 1982, Zhang and Makris 2001, Makris and Konstantinidis 2003, Dimitrakopoulos and De Jong 2012, Makris and Vassiliou 2013 and references therein) have thoroughly investigated the dynamics of rocking. The oscillation frequency of a rocking block is not constant since it depends on the vibration amplitude (Housner 1963). However, in the rocking equation of motion (Housner 1963) the characteristic frequency p, which for a rectangular block is expressed as: $p = \sqrt{(3\mathrm{g})/(4R)}$, represents the dynamic characteristics of the block. Under only horizontal excitation, uplift occurs when $\ddot{u}_g > \mathrm{g}\tan\alpha$ (Zhang and Makris 2001), whereas nominally overturning is captured when the tilt (rocking) angle θ exceeds the slenderness angle α.

Fig. 3b captures the geometric and dynamic characteristics of the ancient columns at the three sites that are investigated herein. Specifically, column AC1 resembles a two-dimensional (2D) analogue of a monolithic column of the Temple of Aphaia, while AC2 and AC3 are 2D analogues of columns of the Temples of Olympian Zeus and the Temple of Poseidon, respectively. Although AC2 and AC3 refer to multidrum columns, herein they are treated as equivalent monolithic blocks. This assumption usually leads to more conservative results (higher values of the peak rocking angle) than analyzing the multidrum column (Konstantinidis and Makris 2005). However, the assumption of monolithic blocks is preferred for reasons of simplicity since complex models are needed for assessing the seismic response of multidrum blocks; this is out of the scope of the present study.

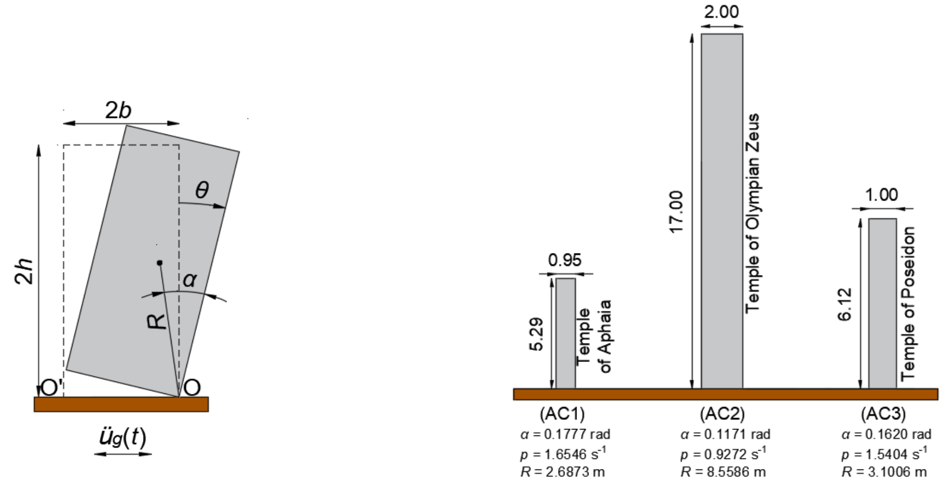

(a) (b)

Fig. 3 – a) Planar rectangular rocking block on a rigid base, b) Dimensions (in meters), geometric, and dynamic characteristics of the three blocks under investigation

By using the simplified 2D rocking model (Housner 1963) and employing Incremental Dynamic Analysis (IDA, Vamvatsikos and Cornell 2002, Lachanas and Vamvatsikos 2022) followed by non-linear regression, Kazantzi et. al 2021 proposed simplified expressions for the parameters (central value and dispersion) of the lognormal rocking fragility functions under ordinary (i.e., no pulse-like no long-duration) ground motions. The derivation of these equations was made by normalizing out the slenderness both in the IM and the engineering demand parameter (EDP). It was found that the seismic response of blocks of different slenderness, but equal size (*p*), tends to be equal to an acceptable degree for practical purposes, especially when rocking is treated under a probabilistic view. For the case of the dimensionless $PGA_{gm}/(\mathrm{g}\tan\alpha)$, denoted here as $PGA_{gm}/\mathrm{g}\tan\alpha$, the proposed expressions for the dimensionless median (I_{A50}) and the dispersion (β_A) of the rocking fragility function given the normalized peak absolute rocking angle $\theta_{\max}$ over the slenderness angle α ($\tilde{\theta} = \theta_{\max}/\alpha$) are:

$$I_{A50}\left(\tilde{\theta}\right) = \begin{cases} C_1 + (1.2 - C_1)(\theta/\tilde{\theta}_1) & \text{for } 0 \le \tilde{\theta} \le \tilde{\theta}_1 \\ \left(\dfrac{\tilde{\theta} + \dfrac{B_1}{100}}{0.1A_1}\right)^{\frac{1}{1.25}} + C_1 & \text{for } \tilde{\theta} \le \tilde{\theta} \le 1 \\ I_{A50,ovt} & \text{for } \quad \tilde{\theta} \ge 1 \end{cases} \tag{1}$$

$$I_{A50,ovt} = A_2 + \frac{B_2}{p^2} \tag{2}$$

$$\beta_A = \begin{cases} A_3 \dfrac{\tilde{\theta}^{B_3}}{e^{\tilde{\theta}}} + C_3 & \text{for } 0 \le \tilde{\theta} \le 0.80 \\ \beta_A(\tilde{\theta} = 0.80) & \text{elsewhere} \end{cases} \tag{3}$$

Table 1. Equations and constants used with Eq. (1)–(3) to define median and dispersion values when using PGA_{gm} as the IM

A_1	B_1	C_1	A_2	B_2
$0.4231p^{2.4974}$	$0.5980p^{2.5666}$	0.9631	1.1398	8.8161
A_3	B_3	C_3		
$0.0529p^3 - 0.4774p^2 + 0.9416p + 0.9226$	$0.0292p^3 - 0.2602p^2 + 0.9622p - 0.2140$	0.1763		

Table 2. Median and dispersion via Eq. (1)–(3) for the three columns under investigation at the three LSs

$\tilde{\theta}$	AC1		AC2		AC3	
	I_{A50}	β_A	I_{A50}	β_A	I_{A50}	β_A
0.15	2.085	0.444	4.248	0.673	2.235	0.470
0.35	3.043	0.607	7.339	0.786	3.344	0.632
1.00	4.360	0.708	11.395	0.753	4.855	0.720

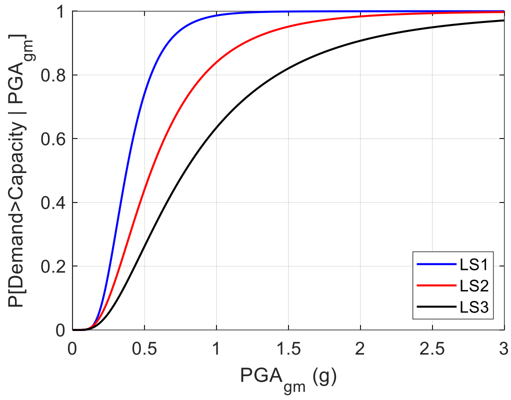

(a) AC1

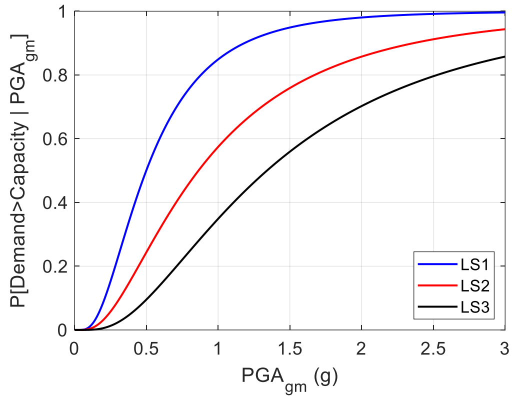

(b) AC2

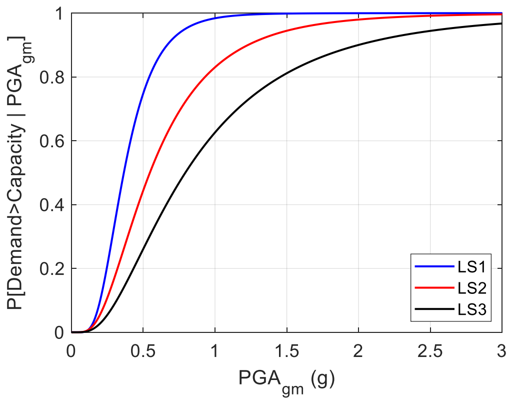

(c) AC3

Fig. 4 – Lognormal fragility curves for the three columns under investigation at the three LSs given PGA_{gm}

Table 1 captures the equations and constants that are used in Eq. (1)–(3). The median and the dispersion are calculated for three $\tilde{\theta}$ thresholds that correspond to the Limit States (LSs) proposed by Psycharis et al. (2013) for classical columns. Specifically, *damage limitation* (LS1) is defined for $\tilde{\theta} = 0.15$, *significant damage* (LS2) for $\tilde{\theta} = 0.35$, and *near collapse* (LS3) for $\tilde{\theta} = 1.00$. Table 2 presents the median and the dispersion via Eq. (1)–(3) for AC1–AC3 for the three limit states. I_{A50} is converted to PGA_{gm} by multiplying with

$g\tan\alpha$ per block, offering the denormalized fragility curves presented in Fig. 3. Column AC2 is significantly taller than the other two columns (Fig. 3b), thus being more stable and showing lower probability of exceeding any of the limit states for any given intensity. The other two columns are of similar slenderness and size (p), showing similar fragility functions. Still, this is only valid under the monolithic assumption for AC3.

4. Seismic risk assessment

The asset risk is assessed on an event-by-event basis by using the IM-fields from the event-based PSHA. For the three cultural heritage sites, both the long-term averages in terms of the MAF of exceeding an LS (λ_{LS}) as well as the probability of exceeding an LS on a scenario-based approach are offered, as detailed in the following.

4.1. Long-term averages

The λ_{LS} for the i-th LS is calculated in each case by taking the full set of IM-fields and summarizing them over the investigation period as:

$$\lambda_{LS_i} = \frac{\sum_{j=1}^{n} P_{exc}[LS_i \mid IM_j]}{t_{eff}} \tag{4}$$

where n is the number of the IM-fields produced from the event-based PSHA, IM_j the IM value of the j-th IM-field (herein in terms of PGA_{gm}), $P_{exc}[LS_i \mid IM_j]$ the probability of exceeding the i-th LS given the j-th IM value taken from the fragility function (Fig. 3) and t_{eff} the effective investigation period (herein 10,000 years). Eq. (4) should be employed carefully when multiple logic tree branches are employed for the event-based PSHA. Results of λ_{LS} can be expressed in terms of the return period of exceedance (T_r) as:

$$T_{r_i} = \frac{1}{\lambda_{LS_i}} \tag{5}$$

Table 3 presents the results in terms of λ_{LS} and T_r for the three sites under investigation. As illustrated, AC1 is of higher seismic risk than the other two columns. This comes from its location in Southwest Attica and thus closer to the large faults that are located in the Corinth Gulf in the West, or Parnitha Mountain in the Northwest. On the other hand, for AC2, the long-term risk of overturning is significantly lower than the other two columns due to the aforementioned more stable behavior.

Table 3. MAF of violating a LS (λ_{LS}) and the corresponding return period T_r via Eq. (4)–(5) for the three columns

LS	λ_{LS} / T_r (years)		
	AC1	AC2	AC3
1	0.0029 / 340	0.0018 / 543	0.0016 / 618
2	0.0018 / 545	0.0008 / 1303	0.0009 / 1057
3	0.0011 / 903	0.0002 / 4681	0.0005 / 1963

4.2. Scenario-based risk assessment

As already mentioned, the main advantage of event-based PSHA is the fact that it produces hazard results that correspond to specific events, offering a view of simultaneous consequences over a spatially distributed portfolio. As an example, a scenario-based risk assessment is performed for three characteristic events taken from the full stochastic set. The epicentres of the selected event are shown in Fig. 5, whereas Table 4 shows per event the exact location of the epicentre (longitude and latitude), the magnitude (M) as well as the PGA_{gm} values that are captured at the three assets under investigation. Of the three events, Event 1 is a potential rupture in the Gulf of Saronikos, Event 2 resembles an extension of the Fili fault system in the area of Aspropyrgos, and Event 3 is a rupture off Cape Sounio, in the Aegean Sea.

Fig. 5 – Location of the epicentre for three potential events close to Attica
(map background from Google Earth, location of assets and epicentres plotted using QGIS)

Table 4. Details of the selected events and the corresponding PGA_{gm} per cultural heritage site under investigation

Event	Epicentre		Magnitude	PGA_{gm} (g)		
	lon.	lat.		Aphaia (AC1)	Olympian Zeus (AC2)	Poseidon (AC3)
1	23.5383	37.8342	6.90	0.618	0.123	0.256
2	23.6544	38.0141	7.10	0.201	1.076	0.134
3	24.0671	37.5370	7.10	0.054	0.076	0.653

Fig. 6, presents the probability of exceeding each LS per column for the three potential events. As shown, on a single event basis the seismic risk may be significantly higher for some columns (e.g., AC3 for Event 3) depending on the location of the epicentre. To this end, although the calculation of the long-term averages returns the summarized risk for each site during the investigation period, the scenario-based approach can be employed as a tool in decision support systems to monitor multiple assets under potential events either frequent or rare.

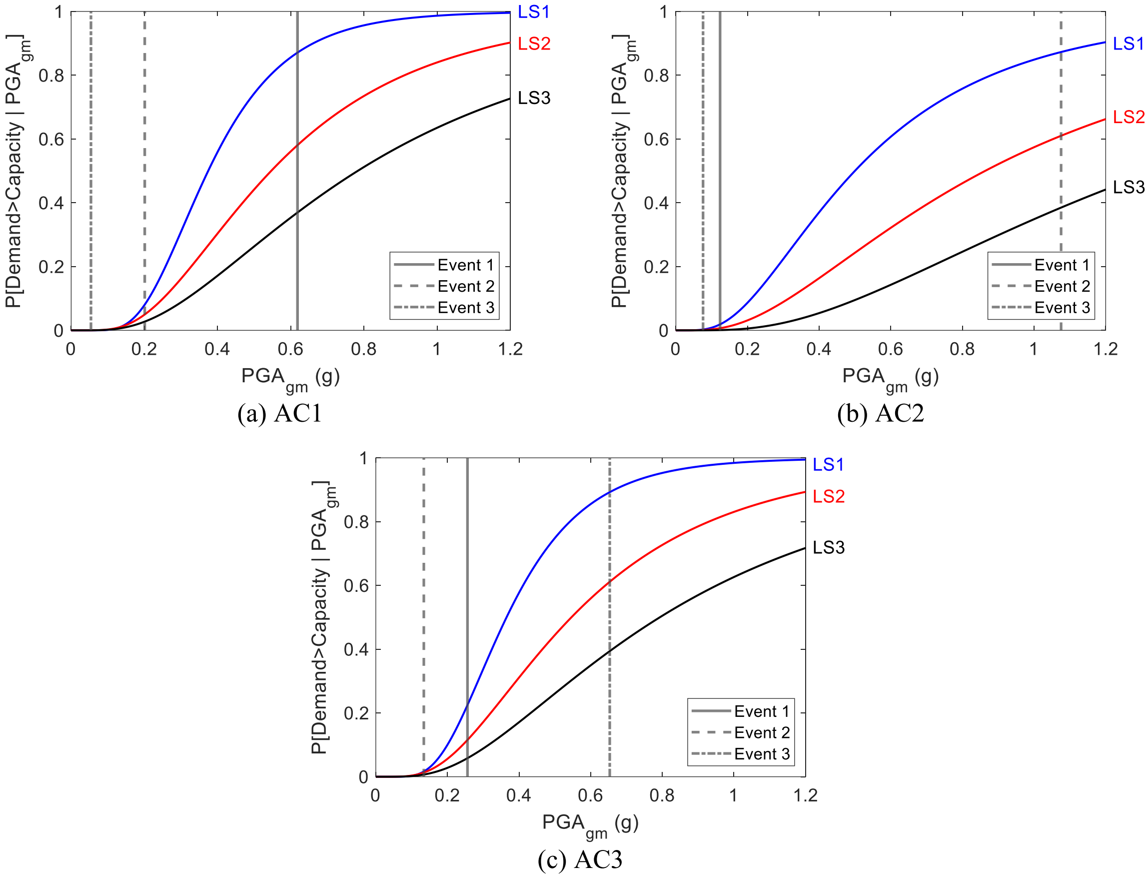

Fig. 6 – Probability of exceeding the three LSs per site for three potential events close to Attica

5. Conclusions

Event-based PSHA offers a powerful basis for portfolio seismic risk assessment since it can produce IM-fields and capture the per-event spatial variability of ground motion hazard. Moreover, simplified models or even expressions for the direct estimation of the distribution parameters for the seismic response offer a fast way for assessing the fragility functions for multiple assets. Without doubt, structure-specific sophisticated structural models will offer a higher level of accuracy, but, at the same time, they need considerably more modelling and computing effort. Hence, either by employing structure-specific models or by treating the model uncertainty as an extra source of uncertainty, the proposed methodology can be easily expanded to cover any set of assets and be incorporated within decision-support systems. This will help the corresponding authorities for prioritizing immediate actions, funding allocation or post-earthquake damage restoration per asset.

Acknowledgements

Research was supported by the Hellenic Foundation for Research and Innovation (H.F.R.I.) under the “2nd Call for H.F.R.I. Research Projects to support Faculty Members & Researchers”, Project "TwinCity: Climate-Aware Risk and Resilience Assessment of Urban Areas under Multiple Environmental Stressors via Multi-Tiered Digital City Twinning", (Number: 2515). Financial support has been also provided by the European Regional Development Fund of the European Union and Greek national funds through the Operational Program Competitiveness, Entrepreneurship and Innovation, under the call RESEARCH – CREATE – INNOVATE (project code: T1EDK-00956), project:

"ARCHYTAS: Archetypal telemetry and decision support system for the protection of monumental structures".

References

Bommer, J.J. (2002). Deterministic vs. probabilistic seismic hazard assessment: an exaggerated and obstructive dichotomy. Journal of Earthquake Engineering, 6: 43–73. https://doi.org9/10.1080/13632460209350432

Boore, D.M., Atkinson, G.M. (2008). Ground-motion prediction equations for the average horizontal component of PGA, PGV, and 5% damped PSA at spectral periods between 0.01s and 10.0s. Earthquake Spectra, 24(1): 99–138. http://dx.doi.org/10.1193/1.2830434

Cornell, C.A. (1968). Engineering seismic risk analysis. Bulletin of the Seismological Society of America, 58(5): 1583–1606.

Dimitrakopoulos, E.G., DeJong, M.J. (2012). Revisiting the rocking block: closed-form solutions and similarity laws. Proceedings of the Royal Society A: Mathematical, Physical and Engineering Sciences, 468(2144): 2294–2318. https://doi.org/10.1098/rspa.2012.0026

Google Earth (2022). https://www.google.com/earth/index.html (last accessed Feb. 2022)

Global Earthquake Model (GEM). (2016). OpenQuake Engine User Instruction Manual, Version 1.9.0, Pavia.

Housner, H. H. (1963). The behavior of inverted pendulum structures during earthquakes. Bulletin of the Seismological Society of America, 53(2): 404–417.

Jayaram, N., Baker, J. W. (2009). Correlation model for spatially distributed ground-motion intensities. Earthquake. Earthquake Engineering and Structural Dynamics, 38(15): 1687–1708. https://doi.org/10.1002/eqe.922

Kazantzi A. K., Lachanas C. G., Vamvatsikos D. (2021). Seismic response distribution expressions for on-ground rigid rocking blocks under ordinary ground motions. Earthquake Engineering and Structural Dynamics, 50(12): 3311–3331. https://doi.org/10.1002/eqe.3511

Konstantinidis, D. Makris, N. (2005). Seismic response analysis of multidrum classical columns. Earthquake Engineering and Structural Dynamics, 34(10): 1243–1270. https://doi.org/10.1002/eqe.478

Lachanas, C. G., Melissianos, V. E., Vamvatsikos, D. (2022). Spatial Variability of Ground Motion Hazard and Preliminary Regional Damage Assessment of Ancient Monuments. In: Vayas I., Mazzolani F.M. (eds) Protection of Historical Constructions. PROHITECH 2021. Lecture Notes in Civil Engineering, vol 209. Springer, Cham. https://doi.org/10.1007/978-3-030-90788-4_49

Lachanas, C. G., Vamvatsikos, D. (2022). Rocking incremental dynamic analysis. Earthquake Engineering and Structural Dynamics, 51(3): 688–703. https://doi.org/10.1002/eqe.3586

Makris, N., Konstantinidis, D. (2003). The rocking spectrum and the limitations of practical design methodologies. Earthquake Engineering and Structural Dynamics, 32(2): 265–289. https://doi.org/10.1002/eqe.223

Makris, N., Vassiliou, M. F. (2013). Planar rocking response and stability analysis of an array of free-standing columns capped with a freely supported rigid beam. Earthquake Engineering and Structural Dynamics, 42(3): 431–449. https://doi.org/10.1002/eqe.2222

Pitilakis, K., Franchin, P., Khazai, B., & Wenzel, H. (Eds.). (2014). SYNER-G: systemic seismic vulnerability and risk assessment of complex urban, utility, lifeline systems and critical facilities: methodology and applications (Vol. 31). ISBN 978-94-007-7872-6, Springer Science+Business Media, Dordrecht

Psycharis, I. N., Fragiadakis, M., and Stefanou, I. (2013). Seismic reliability assessment of classical columns subjected to near-fault ground motions. Earthquake Engineering and Structural Dynamics, 42(14): 2061–2079. https://doi.org/10.1002/eqe.2312

QGIS Development Team (2009). QGIS Geographic Information System. Open Source Geospatial Foundation Project. http://qgis.osgeo.org (last accessed Feb. 2022)

Vamvatsikos, D., Cornell, C. A. (2002). Incremental dynamic analysis. Earthquake Engineering and Structural Dynamics, 31(3): 491–514. https://doi.org/10.1002/eqe.141

Vamvatsikos, D., et al. (2022). The ARCHYTAS Intelligent Decision-Support System for the Protection of Monumental Structures. In: Vayas I., Mazzolani F.M. (eds) Protection of Historical Constructions. PROHITECH 2021. Lecture Notes in Civil Engineering, vol 209. Springer, Cham. https://doi.org/10.1007/978-3-030-90788-4_96

Weatherill, G., Silva, V., Crowley, H., Bazzurro, P. (2015). Exploring the impact of spatial correlations and uncertainties for portfolio analysis in probabilistic seismic loss estimation. Bulletin of Earthquake Engineering, 13(4): 957–981. https://doi.org/10.1007/s10518-015-9730-5

Woessner, J., L. Danciu, D. Giardini, H. Crowley, F., Cotton, G., Grünthal, G., Valensise, R., Arvidsson, R., Basili, M. N., Demircioglu, S., Hiemer, C., Meletti, R. W., Musson, A. N., Rovida, K., Sesetyan, M., Stucchi, and the SHARE consortium. (2015). The 2013 European Seismic Hazard Model: key components and results. Bulletin of Earthquake Engineering, 13(12): 3553–3596. https://doi.org/10.1007/s10518-015-9795-1

Yim, C. S., Chopra, A. K., Penzien, J. (1980). Rocking response of rigid blocks to earthquakes. Earthquake Engineering and Structural Dynamics, 8(6): 565–587. https://doi.org/10.1002/eqe.4290080606

Zhang, J., Makris, N. (2001). Rocking response of free-standing blocks under cycloidal pulses. Journal of Engineering Mechanics (ASCE), 127: 473–483. https://doi.org/10.1061/(ASCE)0733-9399(2001)127:5(473)